Title Page

Intratumoral Delivery of a PD-1-blocking scFv encoded in Oncolytic HSV-1 Promotes Antitumor Immunity and Synergizes with TIGIT Blockade

Chaolong Lin[1#], Wenfeng Ren[1#], Yong Luo[1], Shaopeng Li[1], Yating Chang[1], Lu Li[1], Dan Xiong[1], Xiaoxuan Huang[1], Zilong Xu[1], Zeng Yu[1], Yingbin Wang[1], Jun Zhang[1], Chenghao Huang[1,*], and Ninghshao Xia[1,*]

[1]State Key Laboratory of Molecular Vaccinology and Molecular Diagnostics, National Institute of Diagnostics and Vaccine Development in Infectious Diseases, School of Public Health, Xiamen University, Xiamen, China;

#These authors contributed equally to this work and are co-first authors.

Correspondence:

Chenghao Huang, PhD, School of Public Health, Xiamen University, Xiamen, China, E-mail: huangchenghao@xmu.edu.cn;

Ningshao Xia, School of Public Health, Xiamen University, Xiamen, China, E-mail: nsxia@xmu.edu.cn

The authors declare no potential conflicts of interest.

Running Title: Potentiation of TIGIT blockade by OV expressing a PD-1 scFv

Keywords: oncolytic virus, PD-1-blocking scFv, TIGIT blockade, combination immunotherapy, tumor microenvironment

Abstract

Oncolytic virotherapy can lead to systemic antitumor immunity, but the therapeutic potential of oncolytic viruses (OVs) in humans is limited due to their insufficient ability to overcome the immunosuppressive tumor microenvironment (TME). Here, we showed that locoregional oncolytic virotherapy upregulated the expression of PD-L1 in the TME, which was mediated by virus-induced type I and type II interferons (IFNs). To explore PD-1/PD-L1 signaling as a direct target in tumor tissue, we developed a novel immunotherapeutic herpes simplex virus (HSV), OVH-aMPD-1, that expressed a single-chain variable fragment (scFv) against PD-1 (aMPD-1 scFv). The virus was designed to locally deliver aMPD-1 scFv in the TME to achieve enhanced antitumor effects. This virus effectively modified the TME by releasing damage associated molecular patterns (DAMPs), promoting antigen cross-presentation by dendritic cells, and enhancing the infiltration of activated T cells; these alterations resulted antitumor T cell activity which led to reduced tumor burdens in a liver cancer model. Compared with OVH, OVH-aMPD-1 promoted the infiltration of myeloid-derived suppressor cells (MDSCs), resulting in significantly higher percentages of $CD155^{+}$ G-MDSCs and M-MDSCs in tumors. In combination with TIGIT blockade, this virus enhanced tumor-specific immune responses in mice with implanted subcutaneous tumors or invasive tumors. These findings highlighted that intratumoral immunomodulation with an OV expressing aMPD-1 scFv could be an effective standalone strategy to treat cancers or drive maximal efficacy of a combination therapy with other immune checkpoint inhibitors.

Introduction

Cancer immunotherapy has achieved great therapeutic success over the past several years., only a subset of patients benefit from immunotherapeutic regimens(1). The tumor microenvironment (TME) in many tumor types that do not respond to immunotherapy lacks infiltration of tumor-specific immune cells, lacks neoantigen expression and costimulatory signaling, and exhibits coinhibitory signaling, which restricts the efficacy of cancer therapy(2). Reversing the immunosuppressive TME is the most important challenge in the development of immunotherapeutics(3). Oncolytic viruses (OVs) can selectively replicate in tumor cells and provoke a virus-specific or tumor-specific inflammatory response in the TME(4). OVs can elicit T cell migration to tumor tissue and T cell activation, ultimately mediating local and distant immunotherapeutic efficacy(5). Oncolytic virotherapy is a promising therapeutic strategy for cancer, but further preclinical studies are needed to maximize its therapeutic efficacy(6). The antitumor efficacy of oncolytic virotherapy is significantly enhanced antitumor when combined with systemic immune checkpoint blockade, such as CTLA-4 and PD-1 blockade(7-10). However, this raises several concerns in terms of increased toxicities for patients and medical costs to healthcare systems(11,12). To resolve these issues, investigators have designed various strategies to augment the antitumor immunity of oncolytic virotherapy, such as engineering OVs expressing cytokines, costimulatory factors, and immunomodulatory agents (13-15).

In this study, we analyzed the TME alterations in response to intratumoral virotherapy in order to select a specific immune target to guide our design our multiplexed antitumor

OV vector. We identified that the PD-1/PD-L1 pathway can be targeted to improve an oncolytic herpes simplex virus (OVH), thus constructed a recombinant OVH virus encoding a single-chain variable fragment (scFv) against PD-1 (aMPD-1 scFv), OVH-aMPD-1. We hypothesized that the intratumoral injection of OVH-aMPD-1 would induce potent oncolytic effects and revive intratumoral T cells, inducing antitumor activity. OVH-aMPD-1 increased the infiltration of $CD155^{+}$ myeloid-derived suppressor cells (MDSCs) within the TME. TIGIT blockade improved the antitumor efficacy of OVH-aMPD-1. In summary, we demonstrated that OVH-aMPD-1 exhibited robust antitumor activity and prolonged the survival of tumor bearing mice in multiple different models. This strategy significantly augmented the efficacy of oncolytic virotherapy, providing evidence for the rational design of therapies employing this strategy for clinical investigation.

Materials and Methods

Mice

C57BL/6 mice and BALB/c nu/nu mice were purchased from the Shanghai Slack Laboratory Animal Co., Ltd., bred and housed under specific pathogen-free conditions in the Animal Facility of Xiamen University. The mice used in studies were 4-6 weeks old unless otherwise indicated. All animal protocols were approved by the Institutional Animal Care and Use Committee at Xiamen University for animal welfare (XMULAC20150016).

Cells

HEK293T, Hepa1-6, and U-2 OS cells were purchased from the American Type Culture

Collection (Manassas, VA, 2015). MC38 cells were purchased from the China Infrastructure of Cell Line Resources (Beijing, China, 2018). 293T, U-2 OS and Hepa1-6 cells were cultured in DMEM supplemented with 10% (v/v) fetal bovine serum (FBS) (Invitrogen). MC38 cells were cultured in 1640 medium supplemented with 10% (v/v) FBS. All cells were maintained at 37°C and 5% CO_2. Hepa1-6 PD-L1$^{-/-}$ cells were generated using the CRISPR/Cas9 method. In brief, PD-L1-targeting sgRNAs synthesized by Sangon (Shanghai, China) (sgRNA1 5'- GTATGGCAGCAACGTCACGA -3'; sgRNA2 5'- GCTTGCGTTAGTGGTGTACT -3'; and sgRNA3 5'- GGTCCAGCTCCCGTTCTACA -3'), were cloned into the lentiCRISPR v2 vector (52961, Addgene). HEK293T cells were transfected with packaging plasmids (psPAX2 (12260) and PMD2.G(12259), Addgene) and the lentiCRISPR v2 plasmid by using Lipofectamine 2000 reagent (11668019, Invitrogen) according to the manufacturer's instructions. Virus-containing supernatants were harvested 48 h post transfection. Hepa1-6 cells were transduced with the virus supernatant for 48 h. To obtain PD-L1$^{-/-}$ cells, these cells were stimulated with 20 ng/mL IFN-γ (752806, BioLegend) for 24 h and stained with an anti-PD-L1 antibody (124319, BioLegend), and the PD-L1-negative cells were sorted into single-cell clones. Knockout clones were verified by flow cytometry analysis for PD-L1. Hepa1-6-mRuby3 and MC38-mRuby3 cells were generated by transduction with a lentiviral vector (17477, Addgene) encoding mRuby3 or OVA. Positive clones were selected in culture medium containing 1 μg/ml puromycin (ant-pr-5, InvivoGen), and fluorescent protein expression was confirmed by flow cytometry analysis. Cell lines were not authenticated in the past year and cultured for fewer than 8 passages in indicated medium. All cell lines were

routinely tested using a Mycoplasma contamination detection kit (rep-pt1, InvivoGen).

Viruses and virus generation

OVH was constructed on the backbone of KOS, in which both copies of the ICP34.5 and ICP0 coding sequences were replaced by the eGFP gene and the ICP27 core promoter was replaced with a core hTERT promoter previously constructed in our laboratory. The gene encoding aMPD-1 scFv consisted of a secretion signal sequence (SP), variable light chain (VL), 3×G_4S, variable heavy chain (VK) and His tag (His), which were sequentially amplified from the cDNA sequence of a rat anti-mouse PD-1 antibody (clone 32D6(16)) and assembled into pcDNA3.1 (Invitrogen) under the control of the human cytomegalovirus promoter, named pcDNA3.1-aMPD-1 scFv (Supplemental Fig. S1a and b). OVH-aMPD-1 was constructed on the backbone of OVH, in which both copies of the eGFP coding sequences were replaced by the gene encoding aMPD-1 scFv. OVH-aMPD-1-Luc was constructed on the backbone of OVH-aMPD-1, in which the gene coding luciferase was inserted into the genome between the UL37 and UL38 regions(17). The generation of recombinant virus was performed using a cell-based recombination method as previously described(17).

Virus titration and replication assay

The titers of amplified viruses were determined on U-2 OS monolayers using a classical plaque assay as previously described(18). Viral titers (PFU/ml) were calculated using the following formula: titer = plaque numbers×dilution fold×2. For a virus replication assay, cells were seeded in 6-cm dishes at 10^5 cells/dish and infected with the indicated virus (0.1 PFU/cell) or mock infected. For each time point, the infected cells were harvested and

thereafter subjected to virus titration.

Cytotoxicity assay

In total, 6×10^6 cells were seeded in 6-cm dishes and infected with the indicated virus (1 PFU/cell) or mock infected. For each time point, cell viability was measured by detecting lactate dehydrogenase activity in the lysates using a Cytotoxicity Assay kit (G1780, Promega) according to the manufacturer's instructions.

Western blot analysis

Cell lysates were prepared in RIPA lysis buffer containing a protease inhibitor cocktail (04693132001, Roche), and the protein content of the generated cell lysates was determined using the BCA protein assay (23235, Pierce). Aliquots containing 30 µg of total protein were resolved on a 12% SDS-polyacrylamide gel and transferred to nitrocellulose membrane. After membranes were blocked with 5 % BSA for 1 h, they were probed with indicated primary antibodies overnight at 4 °C, followed by incubation with the HRP-conjugated secondary antibodies (Cell Signaling Technology) for 1 h at room temperature. Finally, the blots were detected with the Lumi-Light^{PLUS} Western blotting Substrate (12015196001, Roche) and images were visualized using the ImageQuant LAS 4000 system (GE Healthcare). Primary antibodies were used for probing: gD (21719, Santa Cruz), ICP0 (56985, Santa Cruz), GFP (32146, Abcam), β-actin (47778, Santa Cruz), cleaved PARP (9541S, Cell Signaling Technology), cleaved Caspase-3 (9664T, Cell Signaling Technology) as well as polyclonal anti-ICP34.5 antibodies.

aMPD-1 scFv expression and purification

For the production of the aMPD-1 scFv recombinant protein, the expression plasmid

pcDNA3.1-aMPD-1 scFv was transfected into HEK293T cells using PEI transfection reagents in Expi293™ Expression Medium (A1435101, Invitrogen). The medium was harvested 5 days after transfection, filtered through a 70-μm nylon filter, concentrated using ammonium sulfate precipitation and stored at 4°C. aMPD-1 scFv was purified by using Ni-NTA chromatography (17-5318-03, GE Healthcare) according to the manufacturer's instructions. aMPD-1 scFv was eluted using 250 mM imidazole and dialyzed in PBS. The purified aMPD-1 scFv was quantified with a BCA assay (23235, Pierce) and stored at −20°C. aMPD-1 scFv proteins were subjected to SDS-PAGE. The proteins separated on the gel were visualized by silver staining (24600, Pierce) according the manufacturer's instructions.

In vitro infection experiments

Cells were cultured in 6-well dishes at 6×10^6 cells/well and infected with OVH at the indicated MOIs. The infected cells were collected for PD-L1 surface labeling at 36 h post infection and analyzed by flow cytometry analysis. The supernatants of the infected and noninfected cells were centrifuged for 5 min at 3000 rpm to remove cellular cell debris. The supernatants from the infected cells were UV inactivated with a UV Stratalinker 2400 instrument (Stratagene, 360 mJ/cm^2) for 5 min, which is sufficient to completely eliminate live virus (Supplemental Fig. S2). For supernatant transfer experiments, the inactivated supernatant was diluted 1:2 in fresh complete medium containing 10% FBS and added to fresh cells in 6-well plates. The infected cells were collected for PD-L1 surface labeling at 24 h post infection and analyzed by flow cytometry. For cytokine treatment, cells were treated with 2,000 U/ml mouse IFN-α (12100, R&D Systems), IFN-γ (485-MI, R&D

Systems), CCL-4 (451-MB, R&D Systems), CCL-9 (463-MG, R&D Systems), IL1α (400-ML, R&D Systems) and TNF-α (410-MT, R&D Systems) for 24 h. For IFNAR blockade, supernatants were treated with an anti-IFNAR antibody (clone MAR1-5A3, BioXcell) at a concentration of 10 μg/ml.

ELISA analysis

The protein expression of aMPD-1 scFv was determined by an indirect chemiluminescence immunoassay (CEIA). Briefly, 96-well plates were coated with 100 ng/well mPD-1-Fc protein (1021-PD, Sino Biological), and nonspecific binding was blocked with PBS containing 20% CBS. Purified aMPD-1 scFv protein, supernatants from OVH-aMPD-1-infected cells, or samples from OVH-aMPD-1-treated mice were added to the wells for a 1-h incubation, followed by washing and reaction with an anti-His-HRP antibody (HRP-66005, Proteintech). After the addition of 100 μl luminol substrates (Wantai BioPharm) for 5 min, the plates were measured with a chemiluminescence reader (ORION II, Berthod). For detection of aMPD-1 scFv in tumors, tumors were weighed and homogenized in 2 mL of sterile PBS in gentleMACS M tubes (130-096-335, Miltenyi Biotec)using a gentleMACS dissociator and with the running program Protein_01 (Miltenyi Biotec). The homogenates were centrifuged for 5 min at 12000 rpm and the supernatants, were assayed using the above method. Empty medium served as a control and serial dilutions of purified aMPD-1 scFv served as standards. The quantity of each experimental sample was determined using a standard curve.

The reactivity of aMPD-1 scFv against PD-1 protein of human origin or mouse origin (Sino Biological) was determined by CEIA as previously described(16). To compare the blocking

activity of the commercial anti-PD1 antibodies (clone RMP1-14 and J43, BioXcell), 32D6 antibodies and aMPD-1 scFv, a blocking CEIA detecting the interaction between his-PD-1 and biotinylated PD-L1 was developed. Briefly, 96-well plates were coated with 50 ng/well of his-PD-1 protein (50124-M08H, Sino Biological), and nonspecific binding was blocked with PBS containing 20% CBS. 32D6 antibody or aMPD-1 scFv was first diluted from 10 μg/ml in PBS containing 5% BSA, followed by two-fold serial dilutions with 8 gradients. Then, a 100 μl dilution or PBS and 100 ng/well biotinylated PD-L1 (71105, BPS Bioscience) was added to the wells for 60 min, followed by washing and reaction with Streptavidin HRP (405210, BioLegend). The plates were assayed using the above method. Control rat isotype IgG added at the same concentration served as a control. The inhibitory ratio was calculated as follows: %inhibitory = 100 × (1 − (average value for each dilution/average value for control)). Each dilution was repeated in triplicate and each test was carried out in triplicate. The results were interpreted by nonlinear, dose-response regression analysis using GraphPad Prism software.

Assays for detecting Interferons

Tumors from vehicle and OVH-treated Hepa1-6 tumors were lysed in RIPA lysis buffer containing a protease inhibitor cocktail (Roche). After clarification by centrifugation for 5 min at 12000 rpm, supernatants were collected, and protein concentrations were normalized by the BCA protein assay (Pierce). IFN-γ, IFN-α and IFN-β concentrations in the supernatants were measured by a mouse IFN-gamma quantikine ELISA Kit (MIF00, R&D Systems), a mouse IFN-alpha ELISA (ab252352, Abcam), and a mouse IFN-beta quantikine ELISA Kit (MIFNB0, R&D Systems), separately, according to the

manufacturer's instructions.

Assays for detecting ICD determinants

MC38 and Hepa1-6 cells were infected with OVH or OVH-aMPD-1 at an MOI of 1 PFU/cell. After 48 h of infection, the cells were collected and stained with an ALEXA FLUOR® 647 conjugated anti-calreticulin antibody (bs-5913R-A647, Bioss) and subjected to flow cytometry to analyze calreticulin-positive cells. Briefly, a monolayer cells was washed with PBS after trypsin digestion, and single-cell suspensions were washed twice with PBS, followed by centrifugation at 1000 rpm for 5 minutes. Cells were then stained with antibodies for 1 h in Brilliant Stain Buffer (563794, BD) on ice in the dark. Following this incubation period, stained cells were washed with PBS and then centrifuged at 1000 rpm for 5 minutes. The supernatant was then aspirated and the resulting cells were resuspended in Brilliant Stain Buffer and samples were run on a BD LSRFortessa X-20 according to manufacturer's recommendations, and data were analyzed by FlowJo 10. The ATP level in the supernatant was measured by the Enhanced ATP Assay Kit (S0027, Beyotime), and the HMGB1 level in the supernatant was measured by an HMGB1 ELISA kit (ST51011, TECAN) according the manufacturer's instructions.

DC purification and phagocytosis assays

To generate bone marrow-derived DCs (BMDCs), single-cell suspensions of bone marrow from wild-type C57BL/6 mice were obtained according to standard protocols with minor modifications(19). Briefly, hind extremities of C57BL/6 mice were collected, soft tissues removed, and bones rinsed in 70% ethanol. After cutting the ends of femurs and tibias, bone marrow was flushed out with RPMI-1640 medium and collected. Red cells were

lysed with RBC lysis buffer (420301, BioLegend). The remaining cells were cultured in RPMI-1640 medium supplemented with 10% FBS, 50 ng/mL GM-CSF (576304, BioLegend) and 25 ng/mL IL-4 (204-IL, R&D Systems) for 7 days. $CD11c^+$ DCs were purified using a Dynabeads™ Mouse DC Enrichment kit (11429D, ThermoFisher) according the manufacturer's instructions. The isolated DCs were cultured overnight with recombinant GM-CSF and Hepa1-6-mRuby3 or MC38-mRuby3 cells pretreated with vehicle or virus for 24 h. The efficiency of DC phagocytosis is expressed as the percentage of $CD11c^+$ $mRuby3^+$ cells among all $CD11c^+$ $CD45^+$ cells, which were counted by flow cytometry analysis.

TIL isolation and flow cytometry analysis

Tumor analysis was performed as previously described(20). For isolation and analysis of TILs, mice were sacrificed, and tumors were harvested for analysis 7 days after two doses of the indicated treatment were given. The tumors were removed using forceps and surgical scissors and weighed. Tumors were minced with scissors and incubated with 1 mg/ml Collagenase D (11088866001, Roche) and 100 μg/ml DNase I (11284932001, Sigma) in RPMI-1640 medium supplemented with 2% FBS for 1.5 h with continuous agitation. The digestion mixture was homogenized by repeated pipetting and filtered through a 70-μm nylon filter. The single cell suspensions were washed twice with a Brilliant Stain Buffer (563794, BD) and stained with the Zombie Aqua™ Fixable Viability Kit (423102, BioLegend) to eliminate dead cells according the manufacturer's instructions. After washing twice, the cells were stained with the corresponding antibodies, incubated for 30 min at 4°C, and then subjected to flow cytometry analysis with a BD LSRFortessa

X-20. Data were analyzed by FlowJo 10. The antibodies used for flow cytometry are listed below: anti-CD45.2 APC/Cy7 (clone 104, 109824), anti-CD3 ε Brilliant Violet 421 (clone 145-2C11, 100341), anti-CD8a Alexa Fluor 700 (clone 53-6.7, 100730), anti-CD11b Brilliant Violet 650 (clone M1/70, 101239), anti-CD11c APC (clone N418, 117310), anti-Ly-6G PE/Cy7 (clone 1A8, 127618), anti-Ly-6C Alexa Fluor® 700 (clone HK1.4, 128024), anti-Gr-1 FITC (clone RB6-8C5, 108406), anti-F4/80 PE/Cy5 (clone BM8, 123112), anti-CD206 PerCP/Cy5.5 (clone C068C2, 141716), anti-CD69 PE (clone H1.2F3, 104508), anti-ICOS PE/Cy7 (clone C398.4A, 313520), anti-CD274 Brilliant Violet 711 (clone 10F.9G2, 124319), anti-CD155 PE (clone 4.24.1, 132205), anti-PD-1 Brilliant Violet 785 (clone 29F.1A12, 135225), and anti-TIGIT PE/Cy7 (clone 1G9, 142108) were obtained from BioLegend; anti-CD4 FITC (clone RM4-5, 553047) was obtained from BD Pharmingen; and anti-mouse CD16/CD32 (14-0161-85) and anti-SIINFEKL/H-2Kb PE (13-5743-82) were obtained from eBioscience.

T cell and tumor cell coculture assay

For coculture of tumor cells and T cells, splenocytes were obtained from wild-type C57BL/6 mice, and T cells were purified from the mouse splenocytes by using the EasySep^{TM} Mouse T Cell Isolation Kit (19851, STEMCELL). Hepa1-6 cells were subjected to 40 Gy of radiation. 5×10^4 irradiated Hepa1-6 cells and were cocultured, without rest, with the T cells in a U-bottom 96-well plate. Anti-CD3/CD28 antibody-coated beads (11456D, Thermo Fisher) and 50 U/ml recombinant mouse IL-2 (51061-MNAE, Sino Biological), together with supernatants from PBS-, OVH-, or OVH-aMPD-1 treated cells or aMPD-1 scFv, were added and incubated with the cells for 120 h. The $CD4^+$ and $CD8^+$ T

287 cells were analyzed using flow cytometry analysis. The IFNγ level in the supernatant was
288 measured by using the mouse IFN-gamma quantikine ELISA Kit (MIF00, R&D Systems)..

289 **Tumor-specific T cells and tumor antigen presentation assay**

290 Tumors or spleens were digested and suspended in a buffer containing 4 μg/ml
291 anti-mouse CD16/CD32 antibodies at a final concentration of 5×10^6 cells/ml. To analyze
292 OVA-specific T cells, single-cell suspensions were stained for 30 min at room temperature
293 with 10 μl of T-Select H-$2K^b$ OVA Tetramer-SIINFEKL-PE (TS-5001-1C, MBL BEIJING
294 BIOTECH) and other indicated antibodies. To analyze cross-presentation by APCs, cells
295 were stained with an anti-SIINFEKL/H-2Kb PE antibody (12-5743-82, eBioscience) at a
296 1:100 dilution for 30 min at 4°C.

297 **Quantitative PCR analysis for HSV-1 DNA**

298 The tumors were removed and weighed. Total DNA was extracted from tumors by
299 QIAamp DNA Blood MiniKit (51106, Qiagen) according to the manufacturer's instructions.
300 DNA content was quantitated using a NanoDrop 2000c Spectrophotometer (Thermo
301 Scientific) and 10 ng of DNA was diluted with nuclease-free water and served as the
302 template for each PCR reaction. Quantitative PCR analysis for HSV-1 DNA was
303 performed using LightCycler® Systems (Roche). The probe consists of forward primers
304 were synthesized by Sangon (Shanghai, China), 5'- GCTGGAACTACTATGACA-3'and
305 reverse primers, 5'-CAGGATAAACTGTGTAATCTC -3' combined with a
306 5'-FAM-TTATCTTCACGAGCCGCAGGT-BHQ-3'-labeled probe specific for the
307 glycoprotein D (gD) gene of HSV-1. Data collected were from a minimum of three
308 experimental replicates all run in at least triplicate. To determine absolute DNA copy

numbers, a standard curve was run in parallel with each analysis using the serial decimal dilutions of gD gene synthesized and quantitated by Sangon (Shanghai, China), and concentrations of HSV-1 DNA in each PCR reaction were expressed as copies of gD gene (Q). The total amounts of HSV-1 DNA in tumors (copies/g tumor) were calculated using the following formula: Q×DNA content/(10ng×tumor weight).

Subcutaneous xenograft model

An inoculum of 5×10^6 Hepa1-6 cells in 100 µl of sterile PBS was injected subcutaneously (s.c.) into the flank of 5-week-old female BALB/c nu/nu mice. After 10 days, the Hepa1-6 tumors reached an average size of ~100 mm^3. The mice were randomized into treatment groups immediately prior to treatment. Virus in 50 µl of sterile PBS was administered via intratumoral injection every three days for three doses in total. Tumor growth was monitored every three days by measurement with a caliper (06-664-16, Fisher Scientific). Twenty-one days after the last treatment, the mice were measured a final time. Tumor volume was calculated according to the formula: (length×$width^2$) /2.

Syngeneic murine cancer model

For the establishment of subcutaneous Hepa1-6 tumors, an inoculum of 5×10^6 murine Hepa1-6 cells or Hepa1-6-OVA cells in 100 µl of sterile PBS was injected s.c. into each flank of 6-week-old female C57BL/6 mice. The mice were randomized into treatment groups on day 7 or 10 following tumor inoculation, immediately before treatment. Virus in 50 µl of sterile PBS was administered via intratumoral injection every three days for three doses in total. Tumor growth was monitored every three days as described above. The overall survival of the mice was monitored over a 90-day period. The tumor-free incidence

is presented as the percentage of tumor-free mice among the total treated mice.

For a mixed competition assay, equal numbers of EGFP- and mRuby3-positive cells were mixed together, and 5×10^6 cells in 100 µl of sterile PBS were injected s.c. into the flank of 6-week-old female C57BL/6 mice. After ten days, when the tumors reached an average size of ~100 mm^3, OVH was administered via intratumoral injection at a dose of 1×10^7 PFU and in 50 µl of sterile PBS. Seven days after virus injection, the percentage of $CD45^-$ fluorescent cells in the tumors was calculated by flow cytometry analysis.

For tumor rechallenge experiments, naive C57BL/6 mice and Hepa1-6 tumor-free C57BL/6 mice treated by virotherapy that survived for 90 days were s.c. rechallenged with 5×10^7 Hepa1-6 cancer cells in the different sites as the primary tumors. The incidence of secondary challenge rejection is presented as the percentage of tumor-free mice among the total rechallenged mice.

For comparing the therapeutic efficacy of OVH plus anti-PD-1 blockers with OVH-aMPD-1 therapy, virus (1×10^7 PFU) and 10 µg of aMPD-1 scFv in 50 µl of sterile PBS was intratumorally injected at day 10 and every 3 days thereafter until three doses were administered.

For combinatorial therapy, virus (1×10^7 PFU) was intratumorally injected in a volume of 50 µl, and 200 µg of anti-Tigit antibody (clone 1G9, BioXcell) or rat IgG isotype control antibodies in 100 µl of sterile PBS were intraperitoneally (i.p.) injected at day 14 and every 3 days thereafter until three doses were administered.

For the establishment of intraperitoneal MC38 tumors, an inoculum of 1×10^6 murine MC38 cells in 200 µl of sterile PBS was injected i.p. into 6-week-old female C57BL/6 mice.

The mice were randomized into treatment groups on day 7 following tumor inoculation, immediately before treatment. Virus (1×10^7 PFU) in 100 µl of sterile PBS and anti-Tigit antibodies (200 µg) in 100 µl of sterile PBS were administered via i.p. injection every three days for three doses in total. The overall survival of the mice was monitored over a 100-day period.

Depletions

Depletion of immune cells was performed with corresponding depleting rat mAbs against different immune markers. When the tumors reached 130 mm^3, all depleting antibodies (anti-CD8α (clone 2.43, BioXcell), anti-CD4 (clone GK1.5, BioXcell) and rat IgG isotype control antibodies) were i.p. administered beginning 2 days before initiation of therapy, at a dose of 400 µg per antibody every two days in 100 µl of sterile PBS for four dosages and thereafter every five days until the end of the experiment. Virus (5×10^6 PFU) in 50 µl of sterile PBS was administered via intratumoral injection into the right flank tumors every three days for three doses in total. The tumor size was monitored for 24 days as described above.

Bioluminescence imaging

Mice that received OVH-aMPD-1 therapy were imaged every day until day 6. Mice were injected retro-orbitally with 50 µl of 40 mg/ml luciferin (E1605, Promega) in PBS and imaged immediately using the IVIS Imaging System (Caliper Life Sciences). Cells infected with OVH-aMPD-1 at different MOIs were incubated with 1ug/mL luciferin in PBS and imaged immediately using the IVIS Imaging System (Caliper Life Sciences).

Immunohistochemistry

375 Tumors were collected at sacrifice and kept in 10% buffered formalin. The fixed tissues
376 were histologically analyzed by immunohistochemistry (IHC) staining of indicated markers.
377 Anti-CD8α (98941)and anti-Ki67 (12202) were obtained from Cell Signaling Technology.
378 Anti-CD155 (LS-B10536) was obtained from LSbio. IHC staining was performed using
379 an Ultrasensitive SP kit (KIT-9720, Maxim) and a DAB detection kit (DAB-0031, Maxim)
380 according to the manufacturer's instructions. Images were taken with a research-level
381 upright microscope (BX51, Olympus) and data were analyzed by cellSens Standard
382 Ver.1.4 software.

383 **Statistics**

384 Statistical significance was calculated using Student's t test or repeated-measure ANOVA,
385 as indicated in the figure legends. Data for survival were analyzed by the log-rank
386 (Mantel-Cox) test. For all statistical analyses, differences were considered significant
387 when the P value was less than or equal to 0.05. (*P < 0.05; **P < 0.01; ***P < 0.001; ****P
388 < 0.0001; ns, not significant). Statistical analyses were performed using GraphPad Prism
389 7. The numbers of animals included in the study are discussed in each figure.

390

391 **Results**

392 **OVH upregulated PD-L1 expression in the TME**

393 To characterize the immunomodulatory effect of intratumoral OVH therapy, we used a
394 Hepa1-6 liver cancer model and analyzed the tumor-infiltrating lymphocytes (TILs) within
395 the tumor tissue after treatment (Fig. 1a). Analysis of virus-injected tumors revealed an
396 increased inflammatory response in the tumors, showing increased infiltration of $CD45^+$

leukocytes and $CD3^+$ lymphocytes (Supplemental Fig. S3, a-c). Notably, there were substantial increases in the absolute numbers of $CD4^+$ and $CD8^+$ T cells (Fig. 1b). $CD45^-$ tumor cells, MDSCs, and dendritic cells (DCs) isolated from the injected and distant tumors had increased expression of PD-L1 (Fig. 1c and d); tumor-associated macrophages (TAMs) isolated from the injected tumors, but not those from distant tumors, also has increased PD-L1 expression (Supplemental Fig. S4a, b and c). Given the existing upregulation of PD-L1 expression with OVH treatment, we chose to explore whether PD-L1 on $CD45^-$ tumor cells could directly attenuate the increased immune response induced by OVH, resulting in the resumption of rapid tumor cell growth. We used a mixed competition assay to test this idea by injecting C57BL/6 mice with mixtures of equivalent numbers of Hepa1-6 wild-type cells that stably expressed mRuby3 and Hepa1-6 PD-L1 knockout (KO) cells that stably expressed EGFP. At 7 days post OVH injection, we measured the cellular composition of the tumors by assessing the fluorescence of the different markers ex vivo (Fig. 1e and Supplemental Fig. S5, a and b). We hypothesized that if PD-L1 was critical for the direct suppression of the $CD8^+$ T cell cytotoxicity mediated by OVH, then the Hepa1-6 PD-L1 KO cells would be selectively depleted. Indeed, the PD-L1 KO cells were selectively reduced in tumors (Fig. 1f). These findings provided rationale for targeting the PD-1/PD-L1 axis directly in tumors, which was further supported by studies demonstrating that PD-L1 blockade can potentiate the efficacy of oncolytic virotherapy(7,8).

OVH-induced type I interferon led to upregulation of PD-L1 in tumor cells

We used GFP-expressing OVH as a tool to investigate the PD-L1 expression of

virus-infected and noninfected cancer cells (Fig. 2a). We found that the infection of mouse tumor cell lines with OVH induced marked PD-L1 upregulation on the surface of both virus-infected and noninfected cells. The intensity of PD-L1 staining was higher in the fraction of virus-infected cells than in that of noninfected cells, suggesting that PD-L1 upregulation was mediated by two mechanisms: direct infection by the virus and an unknown indirect mechanism (Fig. 2b and c). We hypothesized that the upregulation of PD-L1 in noninfected cells after OVH infection was probably mediated by *in situ* secreted immune factors. Therefore, we collected UV-inactivated cell culture supernatants from the infected cells, transferred it to noninfected cells, and detected PD-L1 expression. We found that conditioned medium generated from different cancer cell lines by exposure to virus induced PD-L1 upregulation on the cell surface irrespective of the cancer cell type (Fig. 2d and Supplemental Fig. S6). These findings suggested that secreted immune factors may have promoted the upregulation of PD-L1 expression on other cells in a paracrine fashion. We hypothesized that cytokines may play a major role in PD-L1 upregulation after exposure to OVH, thus treated tumor cells with different cytokines. Treatment of cancer cells with interferons (IFNs) resulted in efficient PD-L1 upregulation, with IFN-γ inducing the most robust PD-L1 upregulation (Fig. 2e and f). To confirm that type I IFN was the regulator of the PD-L1 increase, we treated cells with UV-inactivated cell culture supernatants from infected cells in the presence of an antibody blocking IFNAR or a control antibody. IFN-α, but not IFN-γ, was detected in the transferred supernatants from OVH-infected Hepa1-6 cells (Supplemental Fig. S7a and b). IFNAR antibody blockade resulted in complete abrogation of PD-L1 upregulation by OVH

441 treatment (Fig. 2g), confirming that type I IFN was responsible for the OVH-mediated
442 PD-L1 upregulation observed in vitro. Furthermore, we used tumor cells and a T cell
443 coculture assay to confirm that type II IFN was the regulator of the PD-L1 increase. We
444 cocultured cancer cells with inactivated T cells or activated T cells in the presence of an
445 antibody blocking IFN-γ or a control antibody (Supplemental Fig. S7c). IFN-γ antibody
446 blockade resulted in significantly reduced PD-L1 expression (Fig. 2h). We next sought to
447 determine whether IFN-γ could be induced by OVH in vivo (Fig. 2i). Intratumoral treatment
448 of tumors with OVH resulted in the induction of IFN-γ expression in the treated tumors (Fig.
449 2j). These findings highlighted the idea that OVH-induced IFN responses can drive PD-L1
450 expression and possibly elicit adaptive immune resistance.
451
452 **Generation of a recombinant OVH expressing an scFv against murine PD-1**
453 To target PD-1 directly within tumors, we engineered a recombinant OVH encoding an
454 aMPD-1 scFv (OVH-aMPD-1) (Fig. 3a). The blocking ability of aMPD-1 scFv in inhibiting
455 the interaction between PD-1 and PD-L1 was similar to the other well-known commercial
456 antibodies (RMP1-14 and J43), and aMPD-1 scFv specifically recognized mouse PD-1
457 (Supplemental Fig. S8a and b). The recombinant viruses were verified by examining viral
458 genes and exogenous gene expression (Fig. 3b). Further in vitro characterization of
459 OVH-aMPD-1 revealed that the virus was equivalent to the parental OVH strain in regards
460 to its replicative capacity (Fig. 3c) and cell-killing ability (Fig. 3d) in U-2 OS cells.
461 OVH-aMPD-1 possessed significant cell-killing activity against Hepa1-6 cells and MC38
462 cells (Supplemental Fig. S9). Infection of U-2 OS cells with OVH-aMPD-1 resulted in an

463 over 1,000-fold increase in aMPD-1 scFv in the supernatant of the infected cells in a
464 time-dependent fashion (Fig. 3e). The expression of aMPD-1 scFv was relatively higher in
465 human cancer cells than in mouse cancer cells possibly due to the relatively low
466 permissivity of mouse cancer cells to HSV-1 (Fig. 3f). As expression was most efficient in
467 Hepa1-6 cells, this cell line was selected as the primary model for in vivo studies.
468 Intratumoral administration of OVH-aMPD-1 into Hepa1-6 tumors resulted in significant
469 aMPD-1 scFv expression in treated tumors in a time-dependent fashion (Fig. 3g). Finally,
470 we confirmed the T cell-stimulating property of recombinant aMPD-1 scFv purified from a
471 virus-infected cell culture (Fig. 3h and Supplemental Fig. S10).
472
473 **OVH-aMPD-1 improved DC cell presentation and revived T lymphocytes**
474 Studies indicate that PD-1 expression by TAMs significantly inhibits phagocytosis and
475 antitumor immunity(21), suggesting that PD-1 blockade may restore phagocytosis. We
476 wondered whether aMPD-1 scFv derived from OVH-aMPD-1 infection could promote
477 phagocytosis, and thus we used an in vitro phagocytosis assay to test this idea using DCs.
478 The results revealed that the phagocytosis of cancer cells by DCs was significantly
479 increased when cancer cells were preinfected with virus, and OVH-aMPD-1 induced
480 much stronger phagocytosis than OVH (Fig. 3i and j; Supplemental Fig. S11a). To
481 determine if aMPD-1 scFv secreted from OVH-aMPD-1-infected tumor cells could prevent
482 $CD3^+$ T cells exhaustion by reversing PD-1-mediated immune inhibition, we used
483 Hepa1-6 cells and a T cell coculture assay. Compared to the OVH-treated supernatants,
484 the OVH-aMPD-1-treated supernatants significantly increased the percentages of $CD4^+$

and $CD8^+$ T cells with upregulation of ICOS and CD69 expression (Fig 3k and l). Compared to the OVH-treated supernatants, the OVH-aMPD-1-treated supernatants also significantly increased the IFN-γ secretion of $CD8^+$ T cells (Fig 3m). These in vitro results indicated that aMPD-1 scFv expression from OVH-aMPD-1 led to an enhanced cytotoxic killing ability in T cells.

Next, we asked if OVH-aMPD-1 enhanced phagocytosis could improve presentation by DCs. To analyze cross-presentation by APCs induced by OVH-aMPD-1 in vivo, tumors were harvested as described in Fig. 3n. Our results showed that OVH-aMPD-1 and OVH significantly increased the ability of APCs to cross-present the MHC-I-restricted OVA-derived SIINFEKL peptides (Fig.3o and Supplemental Fig. S11b), which may be conducive to the activation of tumor-specific $CD8^+$ T cells. OVH-aMPD-1 exhibited relatively excellent DC cell presentation in vivo. These results indicated that OVH-aMPD-1 treatment led to improved antigen presentation by DCs.

OVH-aMPD-1 induced immunogenic cell death in murine cancer cells

OVH-aMPD-1-infected tumor cells promoted phagocytosis, thus improving antigen presentation by DCs. To understand why we first dissected the cell death pattern induced by OVs. We tested the activity of the apoptotic executioner caspase-3 and apoptotic marker PARP. The cleaved forms of both markers were increased after either OVH infection or OVH-aMPD-1 infection (Supplemental Fig. S12a), indicating that OV-induced oncolysis could lead to apoptotic cell death. To determine the immunogenicity of OV-treated cancer cell lines, and the infected cells and supernatants were harvested and

analyzed for expression of immunogenic cell death (ICD)-associated damage-associated molecular patterns (DAMPs). The levels of secreted ATP, surface expressed calreticulin, and secreted HMGB1 were upregulated in the OVH-infected cancer cells and OVH-aMPD-1-infected cancer cells (Supplemental Fig. S12, b to d). Our study revealed that OVH and OVH-aMPD-1 both induced ICD in murine cancer cells, thus leading to DC stimulation. We observed OVH-aMPD-1 induced stronger antigen presentation by DCs than OVH, which may be associated with the expression of aMPD-1 scFv.

OVH-aMPD-1 improved tumor control and enhanced effector T cell function

To further evaluate the antitumor potential of OVH-aMPD-1 in vivo, we used a preclinical murine tumor model bearing bilateral Hepa1-6 tumors (Fig. 4a), which were treated with three consecutive intratumoral OV injections. We first excluded the possibility of direct virus infection of untreated tumor on the distant flank (Supplemental Fig. S13, a to g). It was observed that bilateral tumor growth was significantly inhibited both in the OVH-treated group and OVH-aMPD-1-treated group (Fig. 4b and c), and there was no significant difference in tumor size reduction between these two groups. However, more long-term tumor regression was observed in the OVH-aMPD-1-treated group than in the OVH-treated group (Fig. 4d to j). Long-term survivors that rejected primary tumors also rejected a second challenge with a larger amount of Hepa1-6 tumor cells (Fig. 4k). These results showed that OVH-aMPD-1 exhibited relatively excellent therapeutic efficacy in vivo, which led to complete tumor rejection. However, both OVH-aMPD-1 and OVH were comparable in their ability to cause tumor regression in immunodeficient nude mice (Fig.

4l), suggesting that intratumoral aMPD-1 scFv expression from OVH-aMPD-1 led to enhanced therapeutic effects only in immunocompetent tumor models. Additionally, we compared the therapeutic efficacy of OVH plus anti-PD-1 blockers with OVH-aMPD-1 monotherapy. There was no significant difference in therapeutic efficacy between these two groups (Fig. 4m-o), further supporting the benefits of OVH-aMPD1 as a single agent to treat tumor.

To investigate the molecular mechanisms underlying OVH-aMPD-1 mediated tumor control, we analyzed the inflammatory response within tumors (Fig. 5a). Increased infiltration of adaptive cells, including $CD4^+$ and $CD8^+$ lymphocytes, was observed in tumors (Fig. 5b and c), suggesting that abundant immune infiltrates were recruited into the injected tumors and distant tumors treated with either OVH or OVH-aMPD-1. When compared with those isolated from OVH-injected and distal tumors, the $CD4^+$ and $CD8^+$ T cells isolated from the OVH-aMPD-1-injected and distal tumors expressed significantly more of the activation markers ICOS and CD69 (Fig. 5d and e), suggesting that OVH-aMPD-1 enhanced effector T cell function. It seemed that more pronounced $ICOS^+$ $CD8^+$ T cells were infiltrated in the distant tumors compared to the OVH-injected tumors (Fig. 5d and e). These results indicated that OVH-aMPD-1 virotherapy could remodel the TME and lead to the activation of intratumoral T cells.

Despite the significant T cell activation observed after intratumoral administration of OVH-aMPD-1, the magnitude of the effect was dependent on tumor size (Supplemental Fig. S14a and b), suggesting that additional inhibitory mechanisms within the TME prevent complete tumor rejection in large advanced tumor. We carried out IHC staining to

551 analyze the histological changes within the tumor tissue before and after treatment (Fig.
552 5f). OVH and OVH-aMPD-1 treatment induced $CD8^+$ T cells infiltration into the
553 virus-injected tumors and distant tumors (Fig. 5f). Significant upregulation of CD155 and s
554 ignificant reduction in proliferation signals (Ki67) were observed in the virus-injected
555 tumors and distant tumors (Supplemental Fig. S15a and b), which suggested immune
556 mediated tumor inhibition
557
558 **OVH-aMPD-1 potentiated the efficacy of TIGIT blockade**
559 Analysis of TILs from virus-injected and distant tumors revealed that the immune infiltrates
560 were characterized by an increase in $CD11b^+$ $Gr\text{-}1^+$ MDSCs (Fig. 6a and Supplemental
561 Fig. S16a). Significantly higher amounts of MDSCs were observed in both the
562 OVH-aMPD-1-injected and distal tumors compared to the OVH-injected and distal tumors.
563 The percentage of intratumorally $CD155^+$ G-MDSCs and $CD155^+$ M-MDSCs were
564 significantly higher in both the OVH-aMPD-1-injected and distal tumors compared in the
565 OVH-injected and distal tumors (Fig. 6b and c; Supplemental Fig. S17a and b). The
566 upregulation of CD155 expression on tumor cells was not observed in either the
567 OVH-treated group or the OVH-aMPD-1-treated group (Supplemental Fig. S17c).
568 We thus evaluated the efficacy of combination therapy using TIGIT blockade and
569 virotherapy. Combination therapy with OVH-aMPD-1 and an anti-TIGIT antibody led to
570 regression of the virus-injected tumors and distant tumors, which was superior to the
571 combination of OVH and TIGIT blockade (Fig. 6d, e and f). To validate these findings in
572 other tumor models, we used the peritoneal MC38 colon carcinoma model (Fig. 6g).

MC38 cell line exhibited relatively lower sensitivity to OVs infection, resulting in lower expression of aMPD-1 scFv (Fig. 3f and Supplemental Fig. S18). In the MC38 model, the combination of OVH-aMPD-1 and TIGIT blockade was superior to both monotherapies (OVH or TIGIT blockade) and combination therapy (OVH with TIGIT blockade) (Fig. 6h). OVH-aMPD-1 synergized with TIGIT blockade, leading to long-term management of the invasive tumors.

We carried out depletion experiments to analyze whether $CD4^+$ or $CD8^+$ T cells were critical for mediating antitumor effects in non-injected tumors (Fig. 6i and Fig. S19). Depletion of $CD8^+$ T cells or $CD4^+$ T cells in vivo impaired the therapeutic efficacy of combination therapy with OVH-aMPD-1 and an anti-TIGIT antibody (Fig. 6j and k). When $CD8^+$ T cells were depleted in the mice treated with the OV, tumors progressed more rapidly when compared to mice with depletion of CD4+ T cells (Fig. 6j and k). These results demonstrated that $CD4^+$ or $CD8^+$ T cells were critical for mediating tumor regression of both injected tumors and distant tumors.

Combination therapy increased tumor-specific $CD8^+$ T cell responses.

To investigate the immune mechanisms underlying the antitumor efficacy of the combination therapy of TIGIT blockade and OVH-aMPD-1 virotherapy, we used a Hepa1-6-OVA cancer model and analyzed the infiltration of $CD8^+$ T lymphocytes and tumor-specific $CD8^+$ T lymphocytes in tumors and the spleen (Fig. 7a). Increased infiltration of $CD8^+$ T lymphocytes was observed in the tumors treated with either OV, TIGIT blockade or combination therapy (Fig. 7b and c). TIGIT blockade could facilitate

595 $CD8^+$ lymphocyte infiltration regardless of whether OVs were administered, and the
596 percentage of intratumorally infiltrated $CD8^+$ T lymphocytes was significantly higher in the
597 mice receiving combination therapy with TIGIT blockade and OVH-aMPD-1 virotherapy
598 than those receiving combination therapy with TIGIT blockade and OVH virotherapy. In
599 addition, compared with each monotherapy or combination therapy with TIGIT blockade
600 and OVH virotherapy, combination therapy with TIGIT blockade and OVH-aMPD-1
601 virotherapy significantly increased the accumulation of tumor-specific $CD8^+$ T
602 lymphocytes (Fig. 7d and Supplemental Fig. S20). Increased accumulation of
603 tumor-specific $CD8^+$ T lymphocytes was observed in the tumors and spleens isolated from
604 the mice treated with either OVH-aMPD-1 virotherapy or combination therapy with TIGIT
605 blockade and OVH-aMPD-1 virotherapy (Fig. 7e and f). TIGIT blockade could facilitate
606 $CD8^+$ T lymphocyte infiltration into the spleens only when OVH-aMPD-1 was administered,
607 and the percentage of splenic tumor-specific $CD8^+$ T lymphocytes was slightly higher in
608 the mice receiving combination therapy with TIGIT blockade and OVH-aMPD-1
609 virotherapy than in those receiving combination therapy with TIGIT blockade and OVH
610 virotherapy. These in vivo results indicated that aMPD-1 scFv expression from
611 OVH-aMPD-1, together with TIGIT blockade, led to significantly increased numbers of
612 tumor-specific $CD8^+$ lymphocytes, correlating to rejection of established tumors.
613
614 **Discussion**
615 Treatment options and their outcomes in several tumor indications, such as melanoma
616 and small cell lung cancer, have changed significantly. Immunotherapy has become the

first-line therapy for several subsets of patients with a high tumor mutational burden, microsatellite instability or PD-L1 expression, including melanoma, non–small cell lung cancer (NSCLC), colorectal cancer, and urothelial cancer (24). However, the clinical efficacy of immunotherapy is still limited, and a large proportion of patients with advanced cancer do not benefit from current immunotherapeutic strategies(25). Combination therapy with anti-CTLA-4 and anti-PD-1 inhibitors has been suggested as a potential efficacious treatment option for advanced melanoma; however, the potential toxicities of this form of combinatorial immunotherapy is still the largest concern for its clinical application(26,27). There is still an urgent need for improved agents for long-term tumor control. Therefore, the aim of this study was to use an engineered multiplexed OV to improve the potential of oncolytic virotherapy as a standalone therapeutic approach.

Our rationale for constructing an armed OV that can mediate immune checkpoint blockade was that OVH induced strong upregulation of PD-L1 expression in the TME. A similar strategy has been successful in human melanoma patients, where talimogene laherparepvec (T-VEC, armed with GM-CSF) improves antitumor efficacy mediated with GM-CSF-enhancing immune response(28). GM-CSF is an immune stimulator that promotes the differentiation of progenitor cells into DCs and shows a certain degree of antitumor efficacy in clinical trials. The combination of GM-CSF with oncolytic therapy may provide an *in situ* antitumor vaccine by enhancing tumor antigen presentation. Furthermore, intratumoral T-VEC therapy in combination with systemic anti-PD-1 therapy significantly increases overall response rate (62%) in metastatic melanoma patients(10).

639 However, in a randomized open-label phase III trial, 26.4% of the patients in the T-VEC
640 alone arm had an objective response(29). Other studies also suggest that oncolytic
641 virotherapy may improve the efficacy of immune checkpoint blockade by changing the
642 TME(30). These findings highlight that combinatorial regimens can achieve efficacy
643 superior to that of monotherapy. We thus hypothesized that constructing an OV,
644 expressing a PD-1-blocking scFv would provide combinatorial immunotherapy and
645 localized delivery of aMPD-1 scFv in the TME.
646
647 It is intriguing that this antitumor activity was dependent on the expression of aMPD-1
648 scFv within the TME. The limits of this study were the inherent poor replication of
649 OVH-aMPD-1 in murine cancer cells and thus the low production of aMPD-1 scFv in
650 mouse tumors. A major reason for the short-term life cycle of OVH-aMPD-1 in treated
651 mice, which was closely related to the in vivo dynamic kinetics of aMPD-1 scFv
652 expression, is likely to be the relatively low permissiveness of immunocompetent mice,
653 especially C57BL/6 mice, to HSV-1 infection(31,32). This observation suggests that
654 inadequate replication of OVH-aMPD-1 reduces the expression of aMPD-1 scFv and thus
655 restricts combinatorial antitumor effects. Despite this possible replicative defect,
656 compared to its parental virus, OVH-aMPD-1 significantly reduced tumor sizes and
657 extended survival.
658
659 Another possible concern was that aMPD-1 scFv reacted only with PD-1 of mouse origin
660 due to the homology disparity between mouse and human PD-1 sequences, which share

661 approximately 61.1% amino acid identity in the extracellular domains(33). To our
662 knowledge, it is difficult to obtain an antibody that recognizes both human and mouse
663 PD-1 with high affinity and blocking activity, and the activity of an antibody may determine
664 its antitumor activity. Although, aMPD-1 scFv that can bind to PD-1 of both mouse and
665 human origin exists, but whether this aMPD-1 scFv can execute immunomodulatory
666 functions has not been fully addressed(34). For further clinical investigation, we should
667 construct an OV arming with a humanized antibody that recognizes human PD-1.
668
669 In addition to inducing ICD, OVs can induce the release of tumor antigens, which
670 facilitates the initiation of a tumor-antigen specific response within a tumor(35). Our study
671 revealed that OVH-aMPD-1 could not only release immunogenic DAMPs but also
672 significantly promote antigen cross-presentation by DCs. The importance of presentation
673 by DCs in initiating a durable T cell response has previously been demonstrated(36,37),
674 and *in situ* aMPD-1 scFv expression may enhance tumor-antigen specific T cell
675 responses by promoting efficient presentation of antigens to T cells.
676
677 The highly immunosuppressive TME may require a more complex immunotherapeutic
678 strategy(38). Although HSV-1 vectors are emerging as an effective therapeutic approach
679 for cancer, it is ultimately cleared by the host immune system before complete tumor
680 clearance(13). Thus, it is vital to develop rational combinatorial strategies to overcome the
681 highly immunosuppressive TME(39,40). Our rationale for designing combinatorial
682 strategies using OVH-aMPD-1 armed for immune checkpoint blockade was that

683 OVH-aMPD-1 induced significantly higher percentages of $CD155^+$ G-MDSCs and
684 M-MDSCs in tumors. Given that CD155-TIGIT signaling exerts potent inhibitory action in
685 different subsets of immune cells(41,42), this study points toward a promising
686 therapeutic strategy to combine OVH-aMPD-1 with TIGIT blocking agents. Our study
687 revealed that the combination of a virus expressing aMPD-1 scFv with TIGIT blockade
688 significantly improved therapeutic efficacy; however, TIGIT blockade did not improve the
689 antitumor effect of OVH virotherapy. Therefore, *in situ* aMPD-1 scFv expression together
690 with TIGIT blockade further enhanced the locoregional and systemic tumor
691 antigen-specific T cell response. These findings suggest that the magnitude and efficacy
692 of TME remodeling and T cell activation induced by a multifaceted oncolytic vector may
693 potentiate the efficacy of immune checkpoint blockade.
694
695 In summary, our data demonstrated that OVH-aMPD-1 virotherapy was an effective
696 strategy for aMPD-1 scFv delivery and treatment, TME remodeling, improving antigen
697 cross-presentation in DCs and inducing antitumor T cell immunity. To further overcome
698 the highly immunosuppressive TME, OVH-aMPD-1 synergized with TIGIT blockade,
699 which lead to the long-term control of invasive tumors. The findings from this study
700 provide a rationale for the combination of a novel OV armed with immunotherapeutics with
701 immune checkpoint blockade for the treatment of advanced cancer.
702
703 **Acknowledgments**
704 This work was supported by grant 2018ZX10301404-001-002 from the National Science

and Technology Major Project and grant 81571990 from the National Natural Science Foundation of China.

Author Contributions

C.L. and W.R. conducted the experiments; Y.L., Y.C., L.L. and D.X. assisted with virus construction; S.L., X.H., Z.Y., Y.W. and J.Z. assisted with animal experiments; C.H. and N.X. interpreted the data; C.H., N.X. and C.L. designed the experiments and wrote the paper.

References

1. Egen JG, Ouyang W, Wu LC. Human Anti-tumor Immunity: Insights from Immunotherapy Clinical Trials. Immunity **2020**;52(1):36-54 doi 10.1016/j.immuni.2019.12.010.
2. Sharma P, Hu-Lieskovan S, Wargo JA, Ribas A. Primary, Adaptive, and Acquired Resistance to Cancer Immunotherapy. Cell **2017**;168(4):707-23 doi 10.1016/j.cell.2017.01.017.
3. van der Burg SH, Arens R, Ossendorp F, van Hall T, Melief CJ. Vaccines for established cancer: overcoming the challenges posed by immune evasion. Nat Rev Cancer **2016**;16(4):219-33 doi 10.1038/nrc.2016.16.
4. Russell SJ, Barber GN. Oncolytic Viruses as Antigen-Agnostic Cancer Vaccines. Cancer Cell **2018**;33(4):599-605 doi 10.1016/j.ccell.2018.03.011.
5. Lichty BD, Breitbach CJ, Stojdl DF, Bell JC. Going viral with cancer immunotherapy.

Nat Rev Cancer **2014**;14(8):559-67 doi 10.1038/nrc3770.

6. Kaufman HL, Kohlhapp FJ, Zloza A. Oncolytic viruses: a new class of immunotherapy drugs. Nat Rev Drug Discov **2015**;14(9):642-62 doi 10.1038/nrd4663.

7. Engeland CE, Grossardt C, Veinalde R, Bossow S, Lutz D, Kaufmann JK*, et al.* CTLA-4 and PD-L1 checkpoint blockade enhances oncolytic measles virus therapy. Mol Ther **2014**;22(11):1949-59 doi 10.1038/mt.2014.160.

8. Liu Z, Ravindranathan R, Kalinski P, Guo ZS, Bartlett DL. Rational combination of oncolytic vaccinia virus and PD-L1 blockade works synergistically to enhance therapeutic efficacy. Nat Commun **2017**;8:14754 doi 10.1038/ncomms14754.

9. Rajani K, Parrish C, Kottke T, Thompson J, Zaidi S, Ilett L*, et al.* Combination Therapy With Reovirus and Anti-PD-1 Blockade Controls Tumor Growth Through Innate and Adaptive Immune Responses. Mol Ther **2016**;24(1):166-74 doi 10.1038/mt.2015.156.

10. Ribas A, Dummer R, Puzanov I, VanderWalde A, Andtbacka RHI, Michielin O*, et al.* Oncolytic Virotherapy Promotes Intratumoral T Cell Infiltration and Improves Anti-PD-1 Immunotherapy. Cell **2018**;174(4):1031-2 doi 10.1016/j.cell.2018.07.035.

11. Boutros C, Tarhini A, Routier E, Lambotte O, Ladurie FL, Carbonnel F*, et al.* Safety profiles of anti-CTLA-4 and anti-PD-1 antibodies alone and in combination. Nat Rev Clin Oncol **2016**;13(8):473-86 doi 10.1038/nrclinonc.2016.58.

12. Verma V, Sprave T, Haque W, Simone CB, 2nd, Chang JY, Welsh JW*, et al.* A systematic review of the cost and cost-effectiveness studies of immune checkpoint inhibitors. J Immunother Cancer **2018**;6(1):128 doi 10.1186/s40425-018-0442-7.

13. Russell SJ, Peng KW. Oncolytic Virotherapy: A Contest between Apples and Oranges.

749 Mol Ther **2017**;25(5):1107-16 doi 10.1016/j.ymthe.2017.03.026.

750 14. Twumasi-Boateng K, Pettigrew JL, Kwok YYE, Bell JC, Nelson BH. Oncolytic viruses
751 as engineering platforms for combination immunotherapy. Nat Rev Cancer
752 **2018**;18(7):419-32 doi 10.1038/s41568-018-0009-4.

753 15. Wu C, Wu M, Liang M, Xiong S, Dong C. A novel oncolytic virus engineered with
754 PD-L1 scFv effectively inhibits tumor growth in a mouse model. Cell Mol Immunol
755 **2019**;16(9):780-2 doi 10.1038/s41423-019-0264-7.

756 16. Chen Q, Qiu S, Li H, Lin C, Luo Y, Ren W*, et al.* A novel approach for rapid
757 high-throughput selection of recombinant functional rat monoclonal antibodies. BMC
758 Immunol **2018**;19(1):35 doi 10.1186/s12865-018-0274-8.

759 17. Lin C, Li H, Hao M, Xiong D, Luo Y, Huang C*, et al.* Increasing the Efficiency of
760 CRISPR/Cas9-mediated Precise Genome Editing of HSV-1 Virus in Human Cells. Sci
761 Rep **2016**;6:34531 doi 10.1038/srep34531.

762 18. Luo Y, Xiong D, Li HH, Qiu SP, Lin CL, Chen Q*, et al.* Development of an HSV-1
763 neutralization test with a glycoprotein D specific antibody for measurement of
764 neutralizing antibody titer in human sera. Virol J **2016**;13:44 doi
765 10.1186/s12985-016-0508-4.

766 19. Inaba K, Inaba M, Romani N, Aya H, Deguchi M, Ikehara S*, et al.* Generation of large
767 numbers of dendritic cells from mouse bone marrow cultures supplemented with
768 granulocyte/macrophage colony-stimulating factor. J Exp Med **1992**;176(6):1693-702
769 doi 10.1084/jem.176.6.1693.

770 20. Zamarin D, Holmgaard RB, Ricca J, Plitt T, Palese P, Sharma P*, et al.* Intratumoral

modulation of the inducible co-stimulator ICOS by recombinant oncolytic virus promotes systemic anti-tumour immunity. Nat Commun **2017**;8:14340 doi 10.1038/ncomms14340.

21. Gordon SR, Maute RL, Dulken BW, Hutter G, George BM, McCracken MN*, et al.* PD-1 expression by tumour-associated macrophages inhibits phagocytosis and tumour immunity. Nature **2017**;545(7655):495-9 doi 10.1038/nature22396.

22. Banchereau J, Steinman RM. Dendritic cells and the control of immunity. Nature **1998**;392(6673):245-52 doi 10.1038/32588.

23. Savina A, Amigorena S. Phagocytosis and antigen presentation in dendritic cells. Immunol Rev **2007**;219:143-56 doi 10.1111/j.1600-065X.2007.00552.x.

24. Havel JJ, Chowell D, Chan TA. The evolving landscape of biomarkers for checkpoint inhibitor immunotherapy. Nat Rev Cancer **2019**;19(3):133-50 doi 10.1038/s41568-019-0116-x.

25. Topalian SL, Taube JM, Anders RA, Pardoll DM. Mechanism-driven biomarkers to guide immune checkpoint blockade in cancer therapy. Nat Rev Cancer **2016**;16(5):275-87 doi 10.1038/nrc.2016.36.

26. Khalil DN, Smith EL, Brentjens RJ, Wolchok JD. The future of cancer treatment: immunomodulation, CARs and combination immunotherapy. Nat Rev Clin Oncol **2016**;13(5):273-90 doi 10.1038/nrclinonc.2016.25.

27. Sharma P, Allison JP. The future of immune checkpoint therapy. Science **2015**;348(6230):56-61 doi 10.1126/science.aaa8172.

28. Liu BL, Robinson M, Han ZQ, Branston RH, English C, Reay P*, et al.* ICP34.5 deleted

herpes simplex virus with enhanced oncolytic, immune stimulating, and anti-tumour properties. Gene Ther **2003**;10(4):292-303 doi 10.1038/sj.gt.3301885.

29. Andtbacka RH, Kaufman HL, Collichio F, Amatruda T, Senzer N, Chesney J*, et al.* Talimogene Laherparepvec Improves Durable Response Rate in Patients With Advanced Melanoma. J Clin Oncol **2015**;33(25):2780-8 doi 10.1200/JCO.2014.58.3377.

30. Zamarin D, Holmgaard RB, Subudhi SK, Park JS, Mansour M, Palese P*, et al.* Localized oncolytic virotherapy overcomes systemic tumor resistance to immune checkpoint blockade immunotherapy. Sci Transl Med **2014**;6(226):226ra32 doi 10.1126/scitranslmed.3008095.

31. Abghari SZ, Stulting RD, Nigida SM, Jr., Downer DN, Nahmias AJ. Comparative replication of HSV-1 in BALB/c and C57BL/6 mouse embryo fibroblasts in vitro. Invest Ophthalmol Vis Sci **1986**;27(6):909-14.

32. Lopez C. Genetics of natural resistance to herpesvirus infections in mice. Nature **1975**;258(5531):152-3 doi 10.1038/258152a0.

33. Keir ME, Butte MJ, Freeman GJ, Sharpe AH. PD-1 and its ligands in tolerance and immunity. Annu Rev Immunol **2008**;26:677-704 doi 10.1146/annurev.immunol.26.021607.090331.

34. Passaro C, Alayo Q, De Laura I, McNulty J, Grauwet K, Ito H*, et al.* Arming an Oncolytic Herpes Simplex Virus Type 1 with a Single-chain Fragment Variable Antibody against PD-1 for Experimental Glioblastoma Therapy. Clin Cancer Res **2019**;25(1):290-9 doi 10.1158/1078-0432.CCR-18-2311.

35. Bartlett DL, Liu Z, Sathaiah M, Ravindranathan R, Guo Z, He Y*, et al.* Oncolytic viruses as therapeutic cancer vaccines. Mol Cancer **2013**;12(1):103 doi 10.1186/1476-4598-12-103.

36. Hossain DMS, Javaid S, Cai M, Zhang C, Sawant A, Hinton M*, et al.* Dinaciclib induces immunogenic cell death and enhances anti-PD1-mediated tumor suppression. J Clin Invest **2018**;128(2):644-54 doi 10.1172/JCI94586.

37. Palucka K, Banchereau J. Cancer immunotherapy via dendritic cells. Nat Rev Cancer **2012**;12(4):265-77 doi 10.1038/nrc3258.

38. Hughes PE, Caenepeel S, Wu LC. Targeted Therapy and Checkpoint Immunotherapy Combinations for the Treatment of Cancer. Trends Immunol **2016**;37(7):462-76 doi 10.1016/j.it.2016.04.010.

39. Chon HJ, Lee WS, Yang H, Kong SJ, Lee NK, Moon ES*, et al.* Tumor Microenvironment Remodeling by Intratumoral Oncolytic Vaccinia Virus Enhances the Efficacy of Immune-Checkpoint Blockade. Clin Cancer Res **2019**;25(5):1612-23 doi 10.1158/1078-0432.CCR-18-1932.

40. Xu B, Ma R, Russell L, Yoo JY, Han J, Cui H*, et al.* An oncolytic herpesvirus expressing E-cadherin improves survival in mouse models of glioblastoma. Nat Biotechnol **2018** doi 10.1038/nbt.4302.

41. Inozume T, Yaguchi T, Furuta J, Harada K, Kawakami Y, Shimada S. Melanoma Cells Control Antimelanoma CTL Responses via Interaction between TIGIT and CD155 in the Effector Phase. J Invest Dermatol **2016**;136(1):255-63 doi 10.1038/JID.2015.404.

42. Awad RM, De Vlaeminck Y, Maebe J, Goyvaerts C, Breckpot K. Turn Back the TIMe:

Targeting Tumor Infiltrating Myeloid Cells to Revert Cancer Progression. Front Immunol **2018**;9:1977 doi 10.3389/fimmu.2018.01977.

Figure Legends

Figure 1. OVH induced the upregulation of PD-L1 expression in the tumor microenvironment

(a) Treatment scheme for Hepa1-6 hepatoma-bearing mice; s.c., subcutaneously. (b) Absolute numbers of tumor-infiltrating $CD4^+$ and $CD8^+$ T cells isolated from vehicle (PBS) or OVH-injected tumors and distant tumors. (c) Expression of PD-L1 on the surface of $CD45^-$ cancer cells and MDSC cells in tumors. (d) Expression of PD-L1 on the surface of DCs in tumors. (e) Control Hepa1-6 and Hepa1-6 $PD\text{-}L1^{KO}$ tumor cells that stably express mRuby3 or EGFP were mixed at a 1:1 ratio (input) and inoculated s.c. into mice. Representative plots gated on live $CD45^-$ fluorescent cells showing the frequencies of $mRuby3^+$ and $EGFP^+$ cells, among live $CD45^-$ fluorescent cells. (f) Ratio of the frequencies of $mRuby3^+$ and GFP^+ tumor cells in the vehicle or virus-injected tumors.

Triplicates were performed for each experiment and values are the means of three independent experiments (a-f). All values are presented as the mean ± SEM. Statistical analysis was performed using an unpaired two-tailed Student's t tests (b-d); *P < 0.05, **P < 0.01, ***P < 0.001, and ****P < 0.0001.

Figure 2. Upregulation of PD-L1 expression in tumor cells by OVH-induced IFNs

(a) Treatment scheme for OVH infection and PD-L1 analysis. (b) PD-L1 expression in OVH-infected (GFP^+) and noninfected (GFP^-) Hepa1-6 cells (MOI=5). Representative histograms for Hepa1-6 cells and MC38 cells are shown. (c) Quantification of the PD-L1 MFI in different infected cell lines. (d) PD-L1 upregulation in MC38 cells or Hepa1-6 cells treated with UV-inactivated supernatants from vehicle (PBS)-treated or OVH-infected cells (MOI=5). (e) Upregulation of PD-L1 expression in Hepa1-6 cells in response to treatment with recombinant cytokines. (f) Upregulation of PD-L1 expression in MC38 cells in response to treatment with recombinant cytokines. (g) Inhibition of PD-L1 upregulation by an IgG antibody or IFNAR antibody in Hepa1-6 cells treated with UV-inactivated supernatants from vehicle-treated or OVH-infected cells. (h) Inhibition of PD-L1 upregulation by an IgG antibody or IFN-γ antibody in cocultures of either CD3/CD28 antibody-activated T cells or inactivated T cells and Hepa1-6 cells treated with UV-inactivated supernatants from OVH-infected cells. (i) Treatment scheme for IFN-γ detection in tumors in response to OVs treatment. (j) Expression of IFN-γ in vehicle- and OVH-treated Hepa1-6 tumors at 12, 24 and 36 h post treatment. Triplicates were performed for each experiment and values are the means of three independent

881 experiments (b-h). Data represent results from one of three independent experiments with
882 n=5 per group (j). All values are presented as the mean ± SEM. Statistical analysis was
883 performed using one-way ANOVA (c, e-j) or an unpaired two-tailed Student's t test (d); *P
884 < 0.05, **P < 0.01, ***P < 0.001 and ****P < 0.0001..
885
886 **Figure 3. An oncolytic herpes virus expressing a recombinant scFv against murine**
887 **PD-1 (OVH-aMPD-1), improved presentation by DCs and revived T lymphocytes**
888 (a) OVH-aMPD-1 genomic construct scheme. (b) Western blot analysis of various proteins
889 in virus-infected cells. (c) Replication of the parental OVH strain and OVH-aMPD-1 in
890 Hepa1-6 cells. (d) In vitro cell killing of U-2 OS cells by OVH or OVH-aMPD-1 infection. (e)
891 Expression of aMPD-1 scFv in U-2 OS cells at different time points (MOI=1). (f)
892 Expression of aMPD-1 scFv in human and mouse cancer cell lines at 24 h post infection
893 (MOI=1). (g) Expression of aMPD-1 scFv in tumors after OVH or OVH-aMPD-1 treatment,
894 n=6. (h) Activation of T cells by aMPD-1 scFv purified from supernatants of
895 OVH-aMPD-1-infected cells. (i-j) DCs cultured overnight with MC38-mRuby3 or
896 Hepa1-6-mRuby3 cells pretreated with vehicle, OVH or OVH-aMPD-1 for 24 h.
897 Frequencies of $CD11c^+$ $mRuby^+$ MC38 cells (i) and $CD11c^+$ $mRuby^+$ Hepa1-6 cells (j). (k-m)
898 Activated T cells coculture with 5×10^4 irradiated Hepa1-6 cells and supernatants from
899 PBS-, OVH- and OVH-aMPD-1 treated cells at 48 h post infection. The percentages of
900 $CD69^+$ and $ICOS^+$ cells among the $CD4^+$ T cells (k) and $CD8^+$ T cells (l) analyzed by flow
901 cytometry analysis, and the amount of released IFN-γ in the medium (m). (n)
902 Experimental design for analyzing APC cross presentation in vivo. C57BL/6J mice were

903 implanted s.c with Hepa1-6-OVA cells on right flank. Tumors were intratumorally treated
904 with OVs (1×10^7PFU) or PBS (vehicle) for two doses on day 15 and 18. Tumors isolated
905 from mice were dissociated and analyzed by flow cytometry on day 21. (o) The
906 percentages of H-2Kb/SIINFEKL$^+$ cells among the CD11c$^+$MHC-I$^+$ cell population.
907 Triplicates were performed for each experiment and values are the means of three
908 independent experiments (c-m). Data represent results from one of two independent
909 experiments with n=6 per group (o). All values are presented as the mean ± SEM.
910 Statistical analysis was performed using one-way ANOVA (h-m, o)*P < 0.05, **P < 0.01,
911 ***P < 0.001, and ****P < 0.0001.
912
913 **Figure 4. OVH-aMPD-1 improved both local and systemic tumor control**
914 (a) Treatment scheme. (b, c) Growth of vehicle (PBS)-, OVH- and OVH-aMPD-1-treated
915 syngeneic Hepa1-6 tumors in immunocompetent C57BL/6 mice (n=9). Tumor growth of
916 injected (right flank) Hepa1-6 tumors (b) and distant (left flank) Hepa1-6 tumors (c). (d-f)
917 Individual tumor growth curves of vehicle (PBS)-, OVH- and OVH-aMPD-1-injected
918 Hepa1-6 tumors. (g-i) Individual tumor growth curves of distant Hepa1-6 tumors. (j)
919 Percent of tumor free mice in the Hepa1-6 liver cancer model. (k) Survival of cured
920 Hepa1-6 model survivors rechallenged with 5×10^7 Hepa1-6 cells. (l) Growth of vehicle
921 (PBS)-, OVH- or OVH-aMPD-1-treated Hepa1-6 xenografts in immunodeficient nude mice
922 (n=6). Data for survival were analyzed by the log-rank (Mantel-Cox) test (k). (m)
923 Treatment scheme for comparing the therapeutic efficacy of OVH plus anti-PD-1 blockers
924 with OVH-aMPD-1 monotherapy. (n, o) Tumor growth of injected and distant Hepa1-6

tumors. Data either represent results from one of three (b-k) or one of two (l, n, o) independent experiments with n=6 to n=10 per group. All values are presented as the mean ± SEM. Statistical analysis was performed using repeated-measure ANOVA (b, c, l, n, o).*P < 0.05, **P < 0.01, and ***P < 0.001; ns, not significant.

Figure 5. OVH-aMPD-1 enhanced effector T cell function

(a) Treatment scheme. Mice bearing Hepa1-6 tumors were intratumorally injected with vehicle (PBS), OVH or OVH-aMPD-1, and tumors were collected on day 10 post virus injection and analyzed by flow cytometry. The percentages of tumor-infiltrating $CD4^+$ T and $CD8^+$ T cells isolated from the injected (b) and distant tumors (c), gated on the total $CD45^+$ cell population. (d, e) Expression of CD69 and ICOS on the surface of tumor-infiltrating $CD4^+$ and $CD8^+$ T cells in the vehicle-injected or virus-injected tumors (d) and distant tumors (e). (f) IHC analysis of $CD8^+$ T cells marker (CD8α) and CD155 in virus-injected tumor and distant tumor at 7 days after receiving intratumoral injection of two doses of OVH or OVH-aMPD-1 (1×10^7 PFU per dose) or vehicle. Data either represent results from one of three (b-e) or one of two (f) independent experiments with n=5 to n=6 per group. All values are presented as the mean ± SEM. Statistical analysis was performed using one-way ANOVA; *P < 0.05, **P < 0.01, ***P < 0.001, and ****P < 0.0001; ns, not significant.

Figure 6. TIGIT blockade potentiated the efficacy of OVH-aMPD-1 virotherapy

(a) Increase in the proportions of MDSCs in the lymphocyte populations isolated from injected and distant tumors. MDSCs, $CD11b^+$ $Gr\text{-}1^+$ cells. (b, c) Increase in the proportions

of CD155$^+$ G-MDSCs and M-MDSCs in injected tumors (b) and distant tumors (c). G-MDSC, granulocytic-myeloid-derived suppressor cells (CD11b$^+$ Ly6C$^-$ Ly6G$^+$); M-MDSC, monocytic-myeloid-derived suppressor cells (CD11b$^+$ Ly6C$^+$ Ly6G$^-$). (d) Treatment scheme. (e, f) Mice bearing Hepa1-6 tumors received monotherapy or combination therapy. Growth of injected tumors (e) and distant tumors (f). (g) Treatment scheme for establishment of intraperitoneal MC38 tumors. (h) Overall survival was monitored over a 100-day period. (i) Treatment scheme for depletion experiments. (j, k) Mice bearing Hepa1-6 tumors received combination therapy and indicated depletion antibodies or isotype antibodies. Growth of injected tumors (j) and distant tumors (k). Data either represent results from one of three (a-h) or one of two (j, k) independent experiments with n=6 to n=10 per group. Data for survival were analyzed by the log-rank (Mantel-Cox) test (h). All values are presented as the mean ± SEM. Statistical analysis was performed using repeated-measure ANOVA (e, f, j, k) or one-way ANOVA (a-c); *P < 0.05, **P < 0.01, ***P < 0.001, and ****P < 0.0001; ns, not significant..

Figure 7. Combination therapy with TIGIT blockade and OVH-aMPD-1 virotherapy increased tumor antigen-specific CD8$^+$ T cell responses

(a) Treatment scheme. Tumors isolated from mice receiving various treatments were dissociated and analyzed by flow cytometry. (b) Percentages of CD8$^+$ T cells in the live CD45$^+$ cell population. (c) Representative flow cytometry plots of CD45$^+$CD8$^+$ cells gated on the total live CD45$^+$ cell population. (d) Representative flow cytometry plots of OVA-specific (H-2 Kb/SIINFEKL tetramer$^+$) CD8$^+$ cells gated on the CD8$^+$ cell population in the tumor. (e) Percentages of H-2 Kb/SIINFEKL tetramer$^+$ CD8$^+$ T cells in the tumor

969 $CD8^+$ T cell population. (f) Percentage of H-2 Kb/SIINFEKL $tetramer^+$ $CD8^+$ T cells in the

970 splenic $CD8^+$ T cell population. Data either represent results from one of three (b, c) or

971 one of two (d, e, f) independent experiments with n=6 per group. All values are presented

972 as the mean ± SEM. Statistical analysis was performed using one-way ANOVA (b-d); *P <

973 0.05, **P < 0.01, ***P < 0.001, and ****P < 0.0001; ns, not significant..

Figure 1

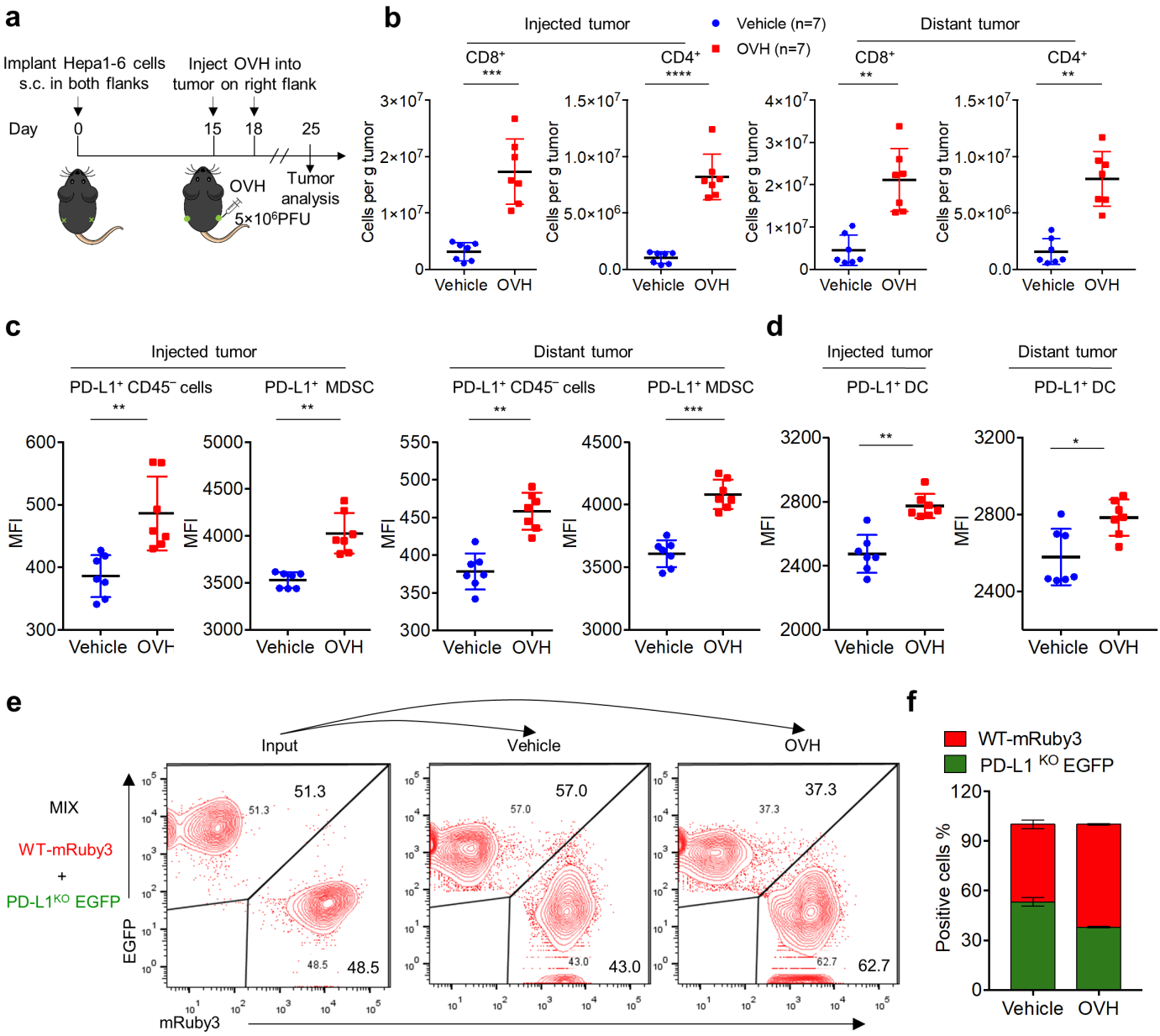

Figure 2

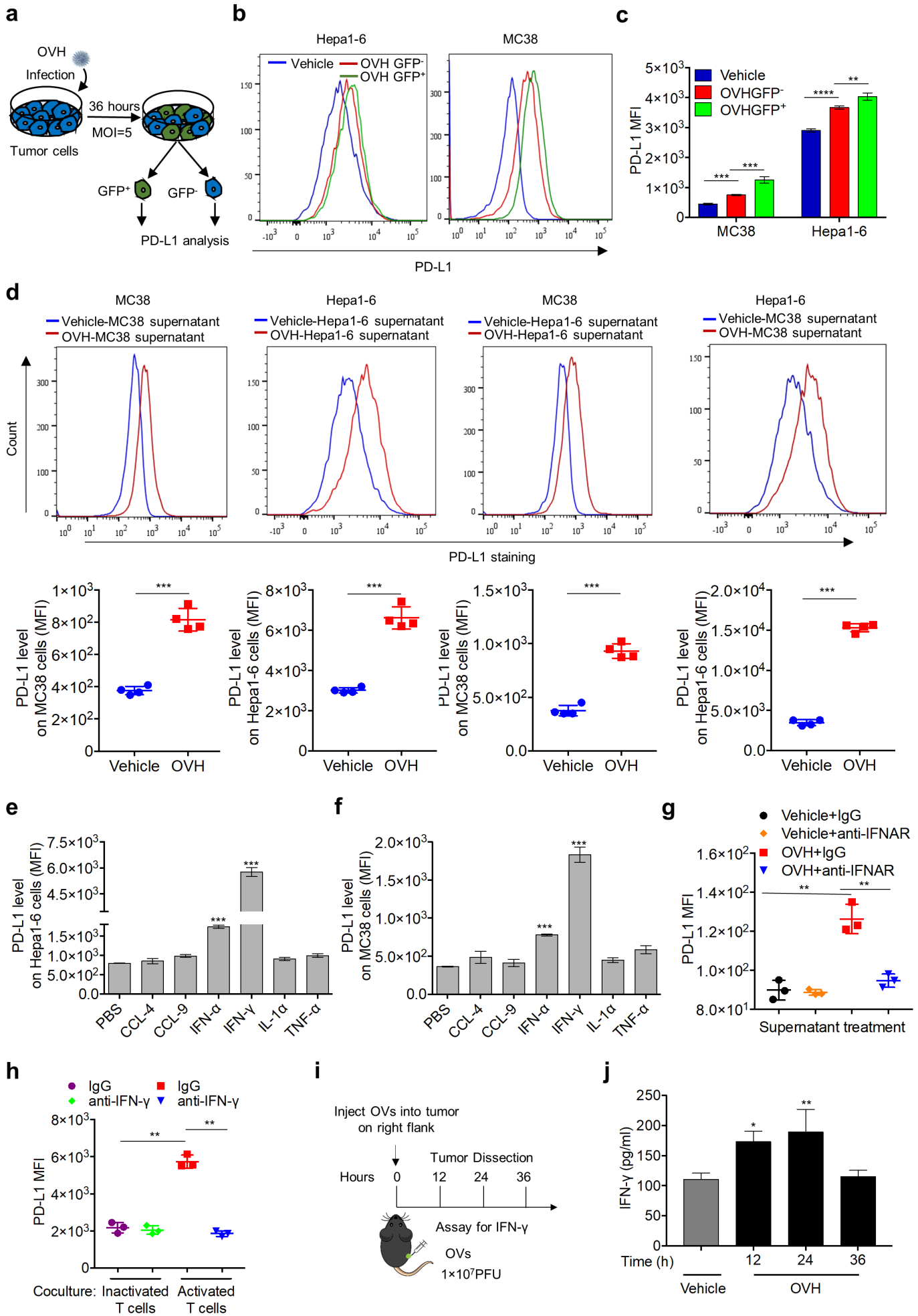

Figure 3

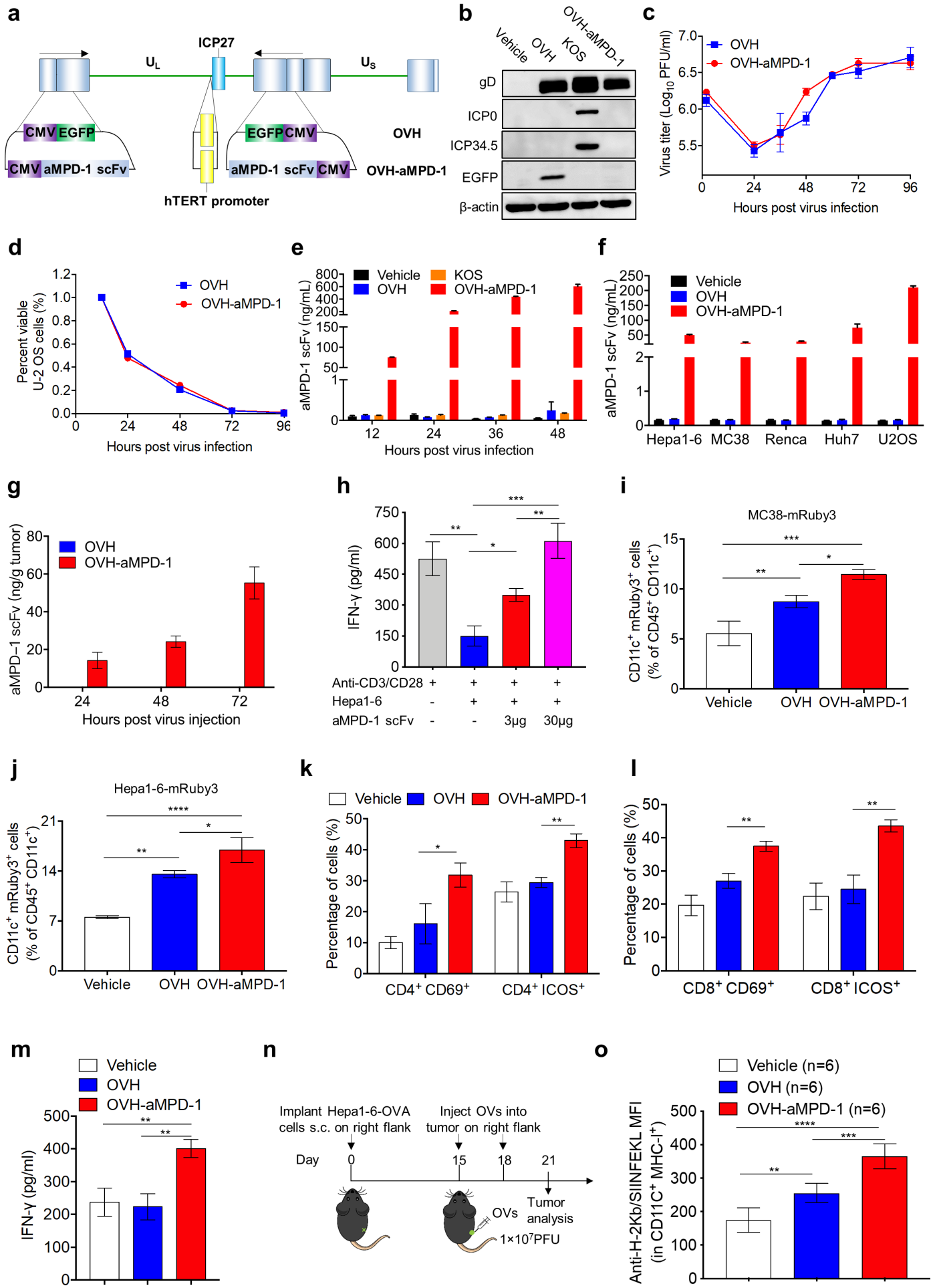

Figure 4

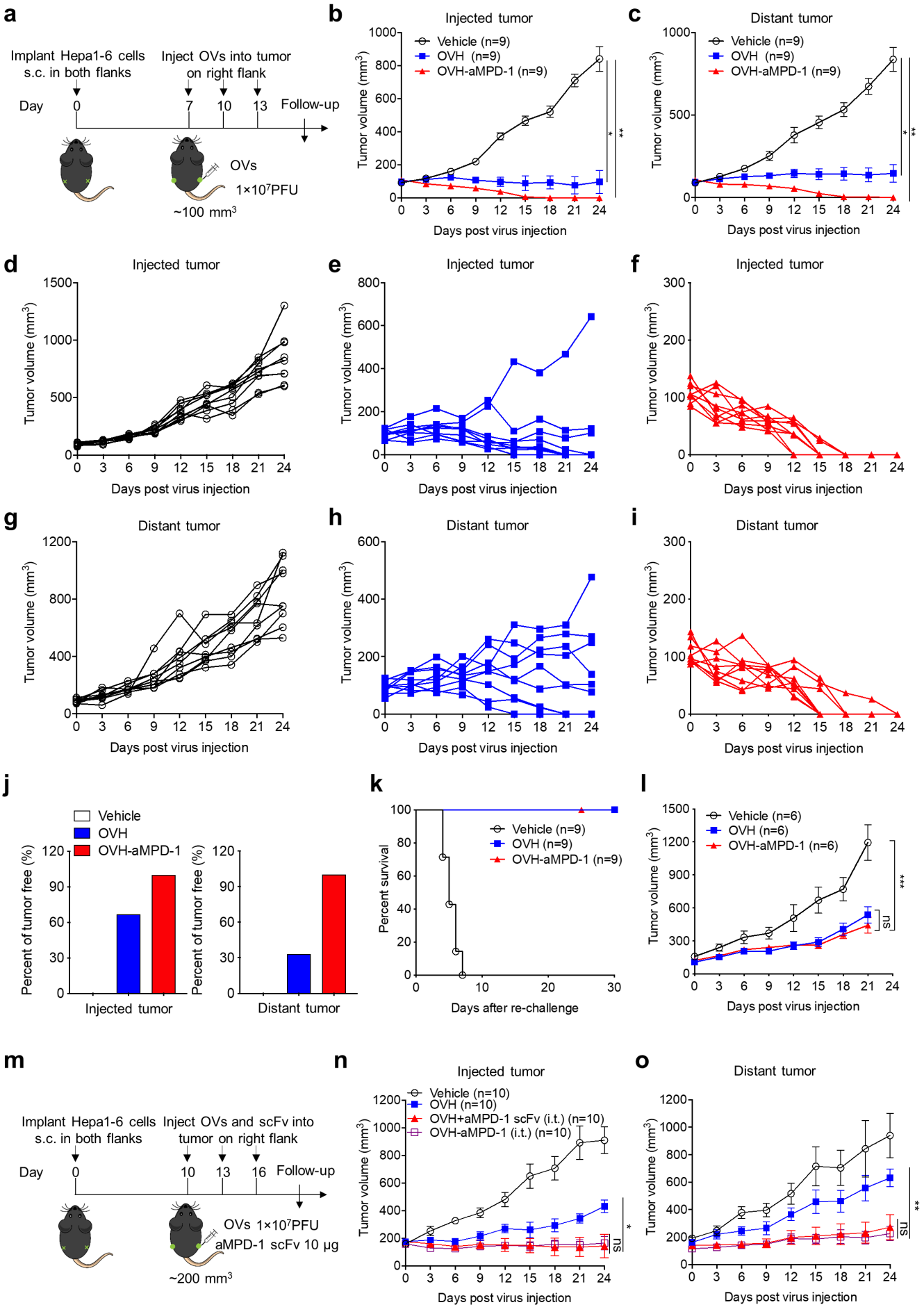

Figure 5

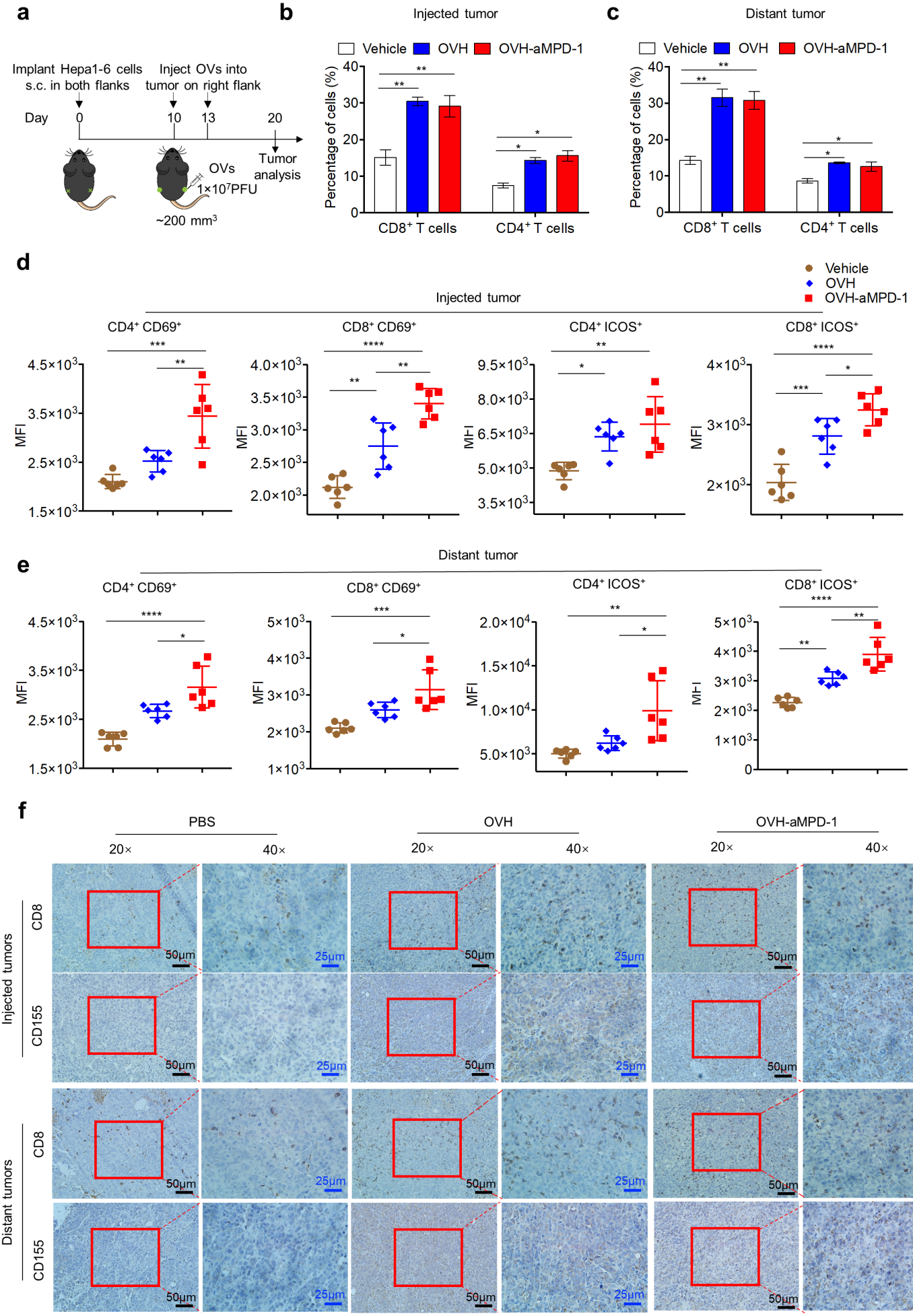

Figure 6

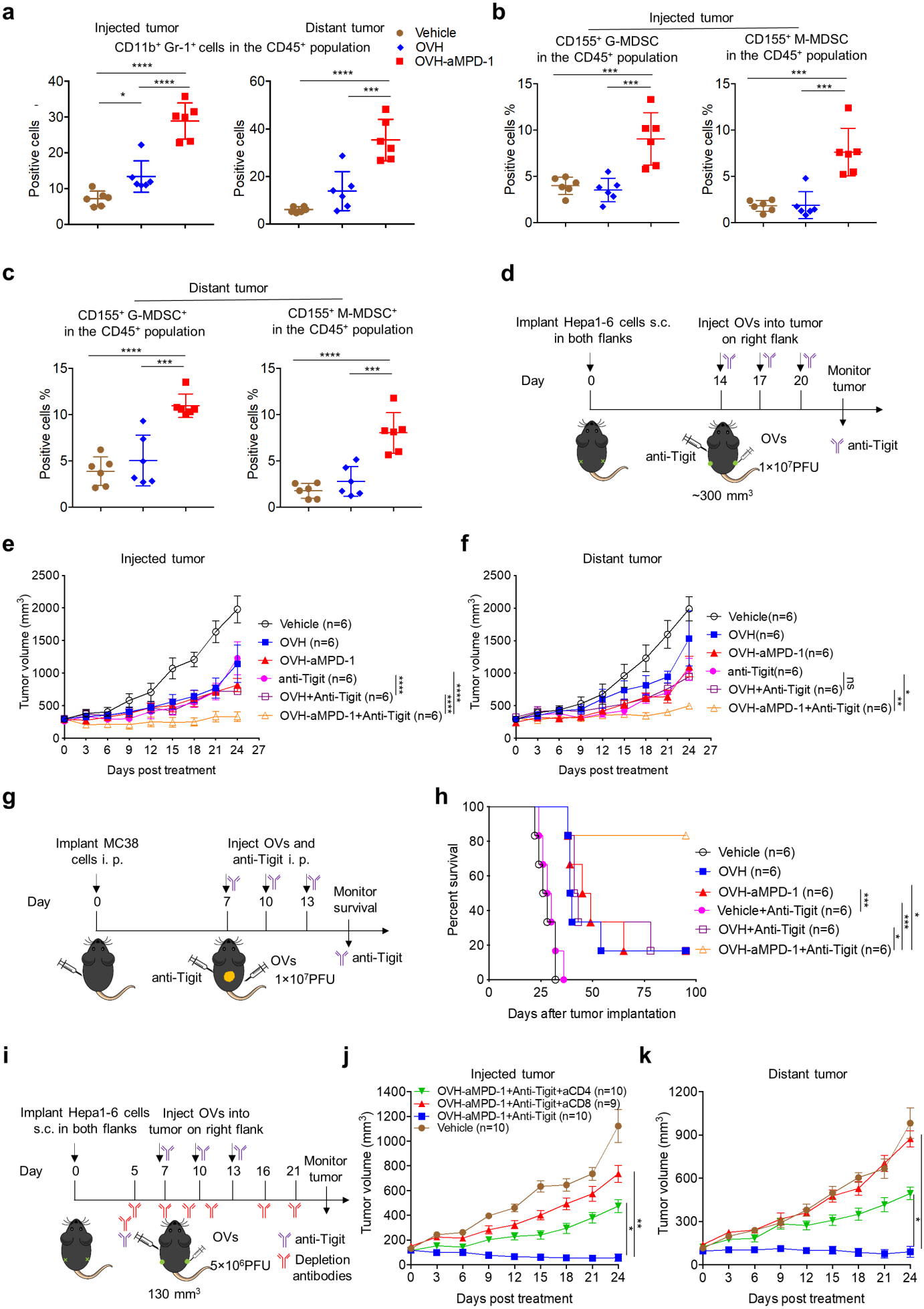

Figure 7

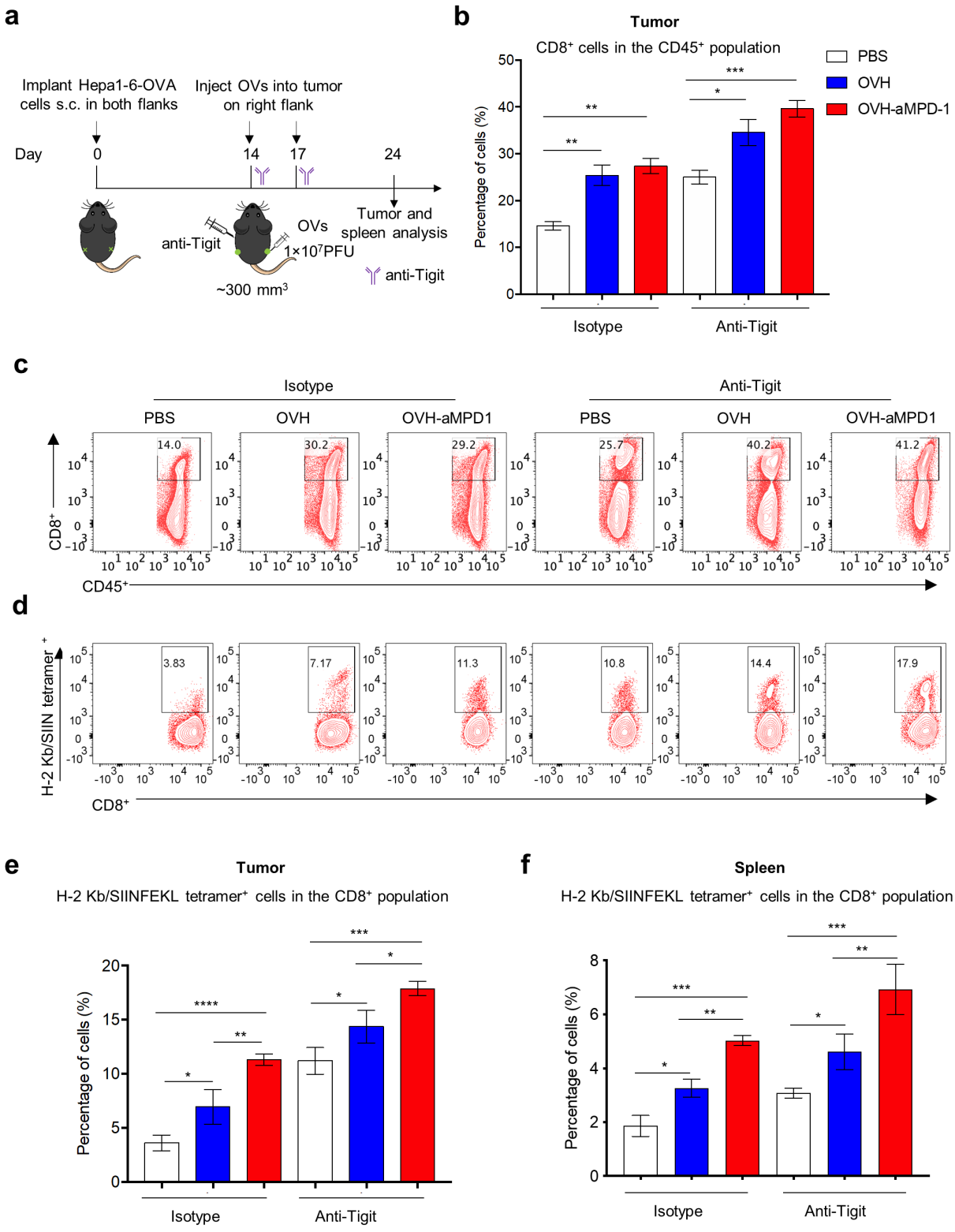

AACR American Association for Cancer Research

Cancer Immunology Research

Intratumoral Delivery of a PD-1-blocking scFv encoded in Oncolytic HSV-1 Promotes Antitumor Immunity and Synergizes with TIGIT Blockade

Chaolong Lin, Wenfeng Ren, Yong Luo, et al.

Cancer Immunol Res Published OnlineFirst March 3, 2020.